How accurate is straw cereal plant density estimation from spectral measurements at early stages

T. Yang, S. Jay, Y. Gao, S. Liu, Frederic Baret

How accurate is straw cereal plant density estimation from spectral measurements at early stages

Tiancheng YANG[1*], Sylvain JAY[1], Yangmingrui GAO[2], Shouyang LIU[2], Frederic BARET[1]
[1]*INRAE, Avignon Université, UMR EMMAH, 84000 Avignon, France*
[2]*PheniX, Academy for Advanced Interdisciplinary Studies, Nanjing Agricultural University, 210095 Nanjing, China*
*tiancheng.yang@inrae.fr

Abstract

This study aimed to estimate the plant density of early straw cereal crops with spectral reflectance for high-throughput phenotyping. Spectral reflectance were collected in microplot experiments from different sites, between 1-leaf to 3-leaf growth stages and with different density treatments. Plant density was estimated indirectly from spectral reflectance using green fraction (GF) as a proxy. The GF values were extracted from RGB images captured at the same time as the spectral measurements. The results show that the estimation with a 45° observation angle with local calibration on different sites and different growth stages had better accuracy (RMSE=82 plants/m^2, rRMSE=0.33) than the others. The band-choosing process showed that using only 4 bands as input resulted in a better balance between model accuracy and simplicity compared to using hundreds of bands.

Keywords: plant density; spectral reflectance; spectral resolution; green fraction (GF).

Introduction

Plant density is a fundamental factor for crop management, and there are at least three reasons: plant density can affect the final yield (Valério et al., 2013); knowing plant density at early stages can help make decisions of field management; and the plant density is a base trait for crop phenotyping.

Many methods have been developed to estimate the density of straw plants in the early stages, with either RGB images or spectral data. These methods can be divided into four categories: (a) segmentation of green pixels and further analysis; (b) deep learning methods used on images; (c) architectural analysis of plants; (d) spectral methods. Among all these four categories, the spectral methods had lower accuracy but could have higher throughput than the others on homogeneous crop fields, because the other methods usually used high-spatial-resolution images. The 45° observation angle was used in other studies because the projected area of plants could be larger, and the small plants were better recognized (Jin et al., 2017; Liu et al., 2017). The 0° and 45° view angles were thus compared in this study.

In this work, spectral reflectance was used to estimate plant density, using GF as a proxy. GF was chosen as the proxy because the relationship between reflectance and GF has been well-studied (Baret et al., 2007; Gitelson et al., 2002), and the relationship between GF and plant density should be proportional when the plants are of similar sizes and have little overlap (Wilke et al., 2021).

Materials and methods

Field experiments and measurements

Microplot experiments were conducted in 2021 and 2022 in five sites in France (Avignon, Salin-de-Giraud, Gardanne, Greoux-les-Bains, and Mauguio), and one site in China (Nanjing) (

Table 1). The size of each microplot was 1 m * 1.4 m in Avignon, Salin-de-Giraud, Gardanne, and Nanjing, while it was 2 m * 12 m in Greoux-les-Bains and 1.36 m * 8 m in Mauguio. These sites had different soil types with different colours. Both dry soil and wet soil were included in the experiments. Three density treatments were set in Avignon, Nanjing, Gardanne, and Salin-de-Giraud. This design resulted in different density values ranging from 37 to 535 plants/m^2, and most density values were between 100 and 450 plants/m^2 (

Table 1). In Avignon, the plants were sown earlier (September) than in the other sites, where more classical sowing dates were used (from October to January). Various cereal crop species (soft wheat, durum wheat, barley, and rye) were considered, as extreme cases of different straw cereal crop cultivars, to explore the possible effects of plant structure on density estimation.

For each location and sowing date, the actual plant density was measured manually at the first date of measurements, and several measurements of spectral and RGB data were made between the one-leaf stage and the three-leaf stage (Table 1). Spectral reflectance measurements were made with the SM-3500 spectrometer (Spectral Evolution, Inc. North Andover, MA 01845 USA), with 737 bands ranging from 343 to 2517 nm. RGB images were collected with digital cameras. In France, a Sony Alpha 5100 camera (Sony, Inc. Minato, Tokyo, Japan.) with 24M pixels, and a 45 mm focal length (in 35 mm equivalent focal length) was used to collect RGB images, and the spatial resolutions of images were between 0.19 and 0.3 mm at the ground level. In China, a Sony RX0 camera with 15M pixels, and a 24 mm focal length (in 35mm equivalent focal length) was used, and the spatial resolutions of images were between 0.25 and 0.5 mm at the ground level. Both the 0° view angle and the 45° view angle were used in the measurements.

Regression methods

GF was used as a proxy in the two-step estimation. In the first step, a gaussian process regression (GPR) model was used to estimate GF from spectral reflectance. The GF values extracted from the deep-learning segmentation of RGB images (GF_rgb) were used as ground truth to calibrate this model (Madec, 2022; Serouart et al., 2022). In the second step, a linear regression model going through the origin was calibrated, taking the estimated GF values as input, and giving plant density values as output.

In both estimation steps, five-fold cross-validation was used in most cases, and leave-one-out cross-validation was used when the dataset was too small. The cross-validation was repeated ten times and the mean result was calculated, to reduce the uncertainty related to the random division of datasets.

Choosing the influential factors and the bands

An ablation study was performed to find out whether the factors of different species, different growth stages, and different sites affected the two relationships of

spectra-GF and GF-density. Sub-models were calibrated with or without differentiating these factors, and overall accuracy values were compared. If the accuracy value significantly increases (or the error significantly decreases) after differentiating one factor, it means that the factor is influential. This ablation study was performed using NIR-RE-R-G-B bands' values as input (842, 717, 668, 560, and 475 nm) for more clarity.

After identifying the most influential factors and the optimal partitioning for model calibration, forward band selection was implemented, using AIC_c (Burnham and Anderson, 2004) as the criteria which considers both the accuracy and parsimony of the model. This process was only applied to spectra-GF estimation. 140 candidate bands were chosen from all 737 bands in 10 nm intervals to speed up the band selection. The band selection started with no band as input. In each loop, the model chose one best band as input from candidate bands, and the "best" band was determined by the lowest AIC_c value of the model. During this procedure, the AIC_c values of different models were recorded. These recorded AIC_c values were compared at last to find out the best number of bands as input. When a comparison between two sets of models was needed, the two sum-AIC_c values of the two sets were compared.

Table 1 Location, date, and species of the experiment. "2.5 leaves" means that the third leaf is not fully expanded, and the third leaf length is about 50% of the second leaf length.

location and sowing date	species	Values of densities (#plant/m2)	number of leaves (date of measurements)
Avignon, France. 2021/9/23	soft wheat, durum wheat, barley	~170; ~340; ~500	1.0 (2021/10/2), 2.0 (2021/10/8), 3.0 (2021/10/15)
Nanjing, China. 2021/11/5	soft wheat, rye, barley	37~330	1.0 (2021/11/22), 2.0 (2021/12/3), 3.0 (2021/12/17)
Greoux-les-Bains, France. 2021/10/28	soft wheat, durum wheat, barley	~250	1.5 (2021/11/18), 2.5 (2021/11/29)
Gardanne, France. 2021/11/19	soft wheat, durum wheat, barley	~150; ~300; ~450	1.5 (2021/1/3), 1.8 (2021/1/11), 3.0 (2021/2/9)
Salin-de-Giraud, France. 2021/11/22	soft wheat, durum wheat, barley	50~400	1.0 (2021/12/20) 1.8 (2021/1/4)
Mauguio, France. 2021/11/19	soft wheat	~300	3.0 (2022/1/7)

Mauguio, France. 2022/1/14	soft wheat	~300	1.5 (2022/2/18)

Results and discussion

Ablation study on the effect of different factors

For the spectra-GF estimation, the ablation study showed the importance of differentiating sites in modelling (Table 2). The strong influence of different sites on the spectra-GF relationship should be because of the difference in soil types and soil colours since the soil greatly impacted the canopy reflectance in the early stages of crop growth.

For the GF_rgb-density estimation, the result is more subtle. Although it had the best accuracy to differentiate all three factors (species, stage, and site), it did not mean that all three factors were of the same importance. Differentiating the stage factor and the site factor already had relatively good accuracy, and these two factors showed a larger impact than the species factor. Further exploration of the images showed that the stage factor and the site factor both affected the architecture of the plant, thus the size of the projected area and finally the GF values. This could change the GF_rgb-density relationship. On the contrary, the species factor showed a limited impact.

As a result, the following spectra-GF estimation models were site-specific, and the GF-density estimation models were site-specific and stage-specific.

Table 2 Comparison of factor combinations for spectral estimation of GF (Spectra→GF) and density estimation based on GF_rgb (GF_rgb→Density). In the Factor-combinations, "Diff-Spc" means "differentiate species", "Diff-Stg" means "differentiate growth stages", and "Diff-Site" means "differentiate sites". The rRMSE values were calculated on the total results of each sub-model.

Factor Combinations			Average rRMSE values in cross-validation (rRMSE_cv, mean±std)			
			Spectra→GF		GF_rgb→Density	
Diff-Spc	Diff-Stg	Diff-Site	0°	45°	0°	45°
√	√	√	0.49	0.43	**0.23**	**0.19**
√	√	×	0.53	0.53	0.44	0.42
√	×	√	0.40	0.34	0.50	0.39
√	×	×	0.51	0.43	0.60	0.52
×	√	√	0.34	0.33	0.28	0.22
×	√	×	0.38	0.38	0.49	0.49
×	×	√	**0.29**	**0.26**	0.52	0.40
×	×	×	0.44	0.38	0.63	0.59

Choosing the bands with AIC_c for spectra-GF estimation

Figure 1 indicated that using 4 bands as input was the best for spectra-GF estimation, in both 0° and 45° view. This selection was determined by the AICc criteria. If fewer than four bands were used, the estimation could be less accurate. On the other hand, if more than four bands were used, any improvement in accuracy was not worth the loss of parsimony in the model.

The chosen bands contained a band close to red (~690 nm) and a band close to red-

edge or near-infrared (~760 nm) for either 0° or 45° view angles (Table 3). These choices were similar to other studies on GF estimation (Baret et al., 1995; Gitelson et al., 1996; Liu et al., 2008), showing the capability of this band selection procedure. However, some chosen bands were rarely used by other studies in GF estimation, such as 397, 1504, and 1791 nm. These bands should be treated with caution because they could come from some random error in the procedure, such as the random splitting of dataset in cross-validation.

A comparison was made between the 0° and 45° observation angles, and 45° was chosen (Table 3). Although the 0° observation had lower RMSE values, that was because of the lower GF values in the nadir view, and the relative error (rRMSE) of the GF estimation was higher. Since the GF values were used as the input of GF-density estimation, the lower rRMSE values were more important and 45° was thus chosen.

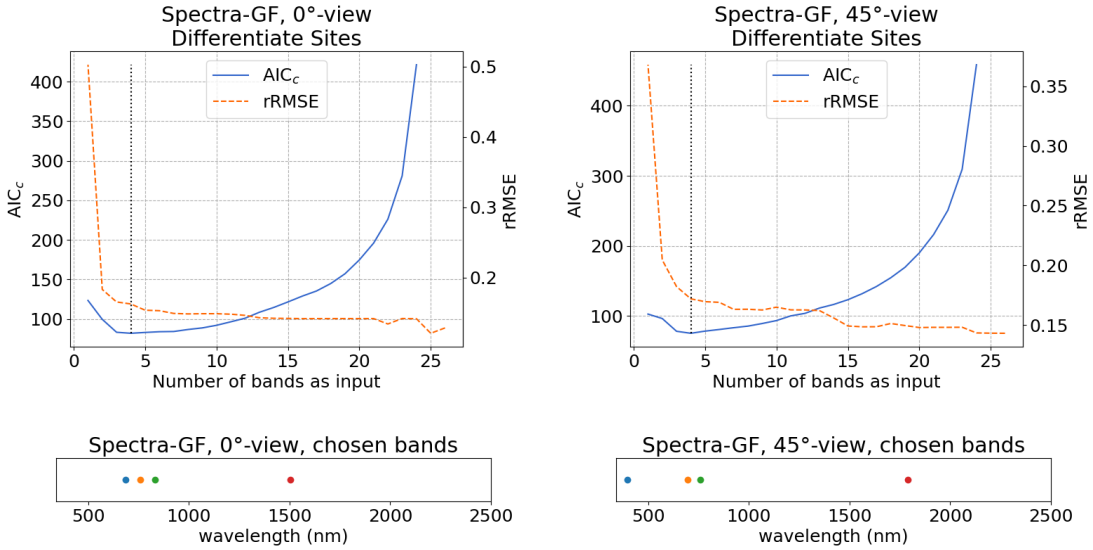

Figure 1 Forward band selection from 140 bands with AIC_c (without cross-validation). The models were calibrated for each site. For 0°-view, chosen bands were 684, 759, 832, and 1504 nm. For 45°-view, chosen bands were 398, 695, 759, and 1791 nm.

Table 3 GF estimation accuracy from models calibrated for each site, with different input bands. The cross-validation was replicated ten times.

Observation angle	wavelengths (nm)	RMSE (mean ± std)	rRMSE (mean ± std)
0°	684, 759, 832, 1504	0.014 ± 0.001	0.29 ± 0.03
45°	397, 695, 759, 1791	0.023 ± 0.003	**0.25 ± 0.03**

Plant density estimation

The result of the plant density estimation is shown in Figure 1, after the local calibration based on the ablation study (Table 2), and with the chosen bands from the band-selection procedure (Figure 1). The RMSE of the estimation was 82 plants/m^2 and the relative error (rRMSE) was 32.6 %. This error was higher than those obtained in other studies based on high-spatial-resolution images, i.e., usually a relative error value of around 10 % (Gnädinger and Schmidhalter, 2017; Jin et al., 2017; Liu et al., 2017; Liu et al., 2020; Wu et al., 2019).

Two reasons could explain the lower accuracy of this study. The first reason was the large variety in the dataset complicated the relationships, while the other studies usually had fewer sites or fewer growth stages. For example, some studies required the observation to be in a specific growth stage to have a better estimation(Jin et al., 2017; Liu et al., 2017), while in this study the large variety revealed the importance of local calibration. The local calibration was based on growth stage and site and shared the same idea with Liu et al. (2018) and Wilke et al. (2021). The second reason was the use of high-spatial-resolution images in other studies greatly improved their accuracy. Methods from thresholding to deep learning benefited from higher spatial resolution, fewer mixed pixels, and the removal of soil pixels. On the contrary, the mining of high-spectral-resolution data remains to be studied.

One important advantage of spectral estimation is the potential in throughput. The spectral estimation will not degrade too much on a homogeneous plot when the pixels become coarser, while the methods based on high-spatial-resolution images were sensitive to the size of pixels (Jin et al., 2017).

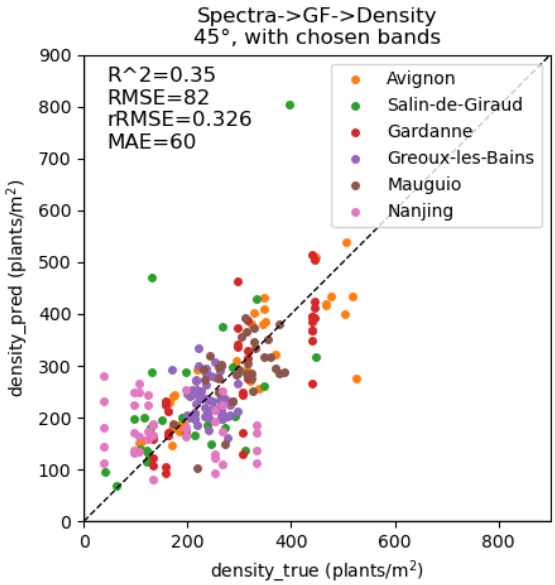

Figure 1 Scatter plot for density estimation. The prediction models were site-specific and stage-specific, and the prediction values for the whole dataset were put together in this plot. The scatter plots correspond to one of the ten replicated calibrations.

Conclusion

Local calibration and band selection enabled the estimation of straw plant density with spectral reflectance data in different sites and species, in early growth stages between the 1-leaf stage and the 3-leaf stage. The accuracy of the two-step estimation was moderate (RMSE=82 plants/m^2, rRMSE=0.326). Differentiating sites improved the spectra-GF estimation while differentiating sites and growth stages were important in the GF-density estimation. Band selection using AICc criteria showed that using four bands as input was better than using hundreds of bands, because using more bands can cause the model to lose parsimony and increase the risk of overfitting. Although the accuracy of the spectral method is lower than methods based on high-spatial-resolution images, the potential of high throughput makes the spectral method promising in

practical use.

Acknowledgement

Among the authors of this article, Tiancheng YANG was funded by the Chinese Scholarship Council. We are very thankful to Gaetan DAUBIGE, Mario SEROUART, Benoit DE-SOLAN, and Vincent MERCIER from ARVALIS and INRAE for helping deploy the experiment in France. We are very thankful to Dong CAI, Chen ZHU, Xiaohai ZHAN, and Ruowen LIU from Nanjing Agricultural University for helping deploy the experiment in China. Thanks to Zengjun QI from Nanjing Agricultural University for providing the seeds of barley. Thanks to Ayoub NACHITE for helping with the code of deep learning segmentation. Thanks to Marie WEISS for helping with the references.

Reference:

Baret, F., Clevers, J., Steven, M., 1995. The robustness of canopy gap fraction estimates from red and near-infrared reflectances: A comparison of approaches. Remote Sensing of Environment 54, 141–151.

Baret, F., Hagolle, O., Geiger, B., Bicheron, P., Miras, B., Huc, M., et al., 2007. LAI, fAPAR and fCover CYCLOPES global products derived from VEGETATION: Part 1: Principles of the algorithm. Remote Sensing of Environment 110, 275–286. https://doi.org/10.1016/j.rse.2007.02.018

Burnham, K.P., Anderson, D.R., 2004. Multimodel inference: understanding AIC and BIC in model selection. Sociological Methods & Research 33, 261–304. https://doi.org/10.1177/0049124104268644

Gitelson, A.A., Kaufman, Y.J., Merzlyak, M.N., 1996. Use of a green channel in remote sensing of global vegetation from EOS-MODIS. Remote Sensing of Environment 58, 289–298.

Gitelson, A.A., Kaufman, Y.J., Stark, R., Rundquist, D., 2002. Novel algorithms for remote estimation of vegetation fraction. Remote Sensing of Environment 80, 76–87. https://doi.org/10.1016/S0034-4257(01)00289-9

Gnädinger, F., Schmidhalter, U., 2017. Digital counts of maize plants by unmanned aerial vehicles (UAVs). Remote Sensing 9, 544. https://doi.org/10.3390/rs9060544

Jin, X., Liu, S., Baret, F., Hemerlé, M., Comar, A., 2017. Estimates of plant density of wheat crops at emergence from very low altitude UAV imagery. Remote Sensing of Environment. 198, 105–114. https://doi.org/10.1016/j.rse.2017.06.007

Liu, J., Miller, J.R., Haboudane, D., Pattey, E., Hochheim, K., 2008. Crop fraction estimation from casi hyperspectral data using linear spectral unmixing and vegetation indices. Canadian Journal of Remote Sensing 34, S124–S138. https://doi.org/10.5589/m07-062

Liu, L., Lu, H., Li, Y., Cao, Z., 2020. High-Throughput Rice Density Estimation from Transplantation to Tillering Stages Using Deep Networks. Plant Phenomics 2020, 1375957. https://doi.org/10.34133/2020/1375957

Liu, S., Baret, F., Andrieu, B., Burger, P., Hemmerle, M., 2017. Estimation of wheat plant density at early stages using high resolution imagery. Frontiers in Plant Science 8, 739. https://doi.org/10.3389/fpls.2017.00739

Liu, T., Yang, T., Li, C., Li, R., Wu, W., Zhong, X., et al., 2018. A method to calculate the number of wheat seedlings in the 1st to the 3rd leaf growth stages. Plant Methods 14, 101. https://doi.org/10.1186/s13007-018-0369-5

Madec, S., 2022. VegAnn: Vegetation Annotation of a large multi-crop RGB Dataset acquired under diverse conditions for image segmentation. Version 1. Non-peer reviewed dataset at https://doi.org/10.5281/zenodo.7126653

Serouart, M., Madec, S., David, E., Velumani, K., Lozano, R.L., Weiss, M., et al., 2022. SegVeg: Segmenting RGB images into green and senescent vegetation by combining deep and shallow methods. Non-peer reviewed preprint at https://www.biorxiv.org/content/10.1101/2022.03.24.485604v1.

Valério, I.P., Carvalho, F.I.F. de, Benin, G., Silveira, G. da, Silva, J.A.G. da, Nornberg, R., et al, 2013. Seeding density in wheat: the more, the merrier? Scientia Agricola 70, 176–184. https://doi.org/10.1590/S0103-90162013000300006

Wilke, N., Siegmann, B., Postma, J.A., Muller, O., Krieger, V., Pude, R., et al., 2021. Assessment of plant density for barley and wheat using UAV multispectral imagery for high-throughput field phenotyping. Computers and Electronics in Agriculture 189, 106380. https://doi.org/10.1016/j.compag.2021.106380

Wu, J., Yang, G., Yang, X., Xu, B., Han, L., Zhu, Y., 2019. Automatic Counting of in situ Rice Seedlings from UAV Images Based on a Deep Fully Convolutional Neural Network. Remote Sensing 11, 691. https://doi.org/10.3390/rs11060691